

Retinal neurovascular responses to transcorneal electrical stimulation measured with optical coherence tomography

Xiaofan Su^{1,*}, Hao Zheng^{1,*}, Qian Li^{1,2}, Pengcheng Sun¹, Meixuan Zhou¹, Heng Li¹, Jiahui Guo¹, Xinyu Chai¹ and Chuanqing Zhou^{1,3} 

¹School of Biomedical Engineering, Shanghai Jiao Tong University, Shanghai 200240, China; ²Center for Medical Physics and Biomedical Engineering, Medical University of Vienna, Vienna 1090, Austria; ³Institute of Biomedical Engineering, Shenzhen Bay Laboratory, Shenzhen 518055, China

*These authors contributed equally to this work.

Co-corresponding authors: Chuanqing Zhou. Email: zhoucq@sjtu.edu.cn; Xinyu Chai. Email: xychai@sjtu.edu.cn

Impact statement

Noninvasive transcorneal electrical stimulation (TES) has emerged as an effective treatment for certain retinal and optic nerve diseases owing to its neuroprotective effects. However, the retinal neurovascular responses evoked by TES have not been completely determined. To investigate this issue, we utilized a custom-designed spectral-domain optical coherence tomography (SD-OCT) to record the retinal neural and vascular responses evoked by TES *in vivo* simultaneously. The present study suggested that TES mainly elicited neural responses in retina, while no significant vascular responses were evoked. Our results provide experimental evidence to the mechanism of retinal neurovascular coupling evoked by TES. Additionally, the present study also suggests that SD-OCT could be utilized as a promoting method to explore neurovascular responses under retinal electrical stimulation.

Abstract

Noninvasive transcorneal electrical stimulation (TES) has emerged as a potential strategy to facilitate visual restoration and promote retinal cell survival for certain retinal and optic nerve diseases owing to its neuroprotective effects. However, the neurovascular responses of retinal neurons evoked by TES have not been completely determined. To investigate this issue, we utilized a custom-designed spectral-domain optical coherence tomography (SD-OCT) to record the retinal neural and vascular responses under TES *in vivo* simultaneously. Significant increases of both positive and negative intrinsic optical signal (IOS) changes were recorded in all three segmented retinal layers, which mainly related to neural activities. However, the changes of TES-induced retinal vascular responses, including blood velocity, cross-sectional area of vessel, and blood flow, were not significant. It suggests that TES mainly elicited neural responses in retina, while no significant vascular responses were evoked. Our results provide experimental evidence to the mechanism of retinal neurovascular coupling under TES. Additionally, the present study also suggests that SD-OCT could be utilized as a promoting method to explore neurovascular responses under retinal stimulation in clinical treatment and technology.

Keywords: Transcorneal electrical stimulation, intrinsic optical signal, neurovascular response, retina, optical coherence tomography

Experimental Biology and Medicine 2020; 245: 289–300. DOI: 10.1177/1535370219900495

Introduction

Neurovascular coupling, which refers to the spatial and temporal relationships between local neural activities and subsequent vascular responses, was first proposed by Roy and Sherrington over 100 years ago.¹ Retina, the only part of the central nervous system that can be visualized noninvasively, also contains neurovascular coupling and provides the unique opportunity to study neurovascular

coupling and related physiological phenomena.² To be specific, the retina consists of several layers of neurons interconnected by synapses, which form the complex neural network to accomplish the preprocessing of visual signals.³ Many retinal diseases, such as age-related macular degeneration,⁴ diabetic retinopathy,⁵ retinitis pigmentosa,⁶ and glaucoma,⁷ are caused by dysfunction in a specific retinal layer, leading to morphological abnormalities or damage in

neurovascular system. Consequently, it is of great significance to detect mechanism of retinal neurovascular coupling for the early diagnosis and treatment of retinal diseases in clinical study.

In recent years, various technologies have been used to detect neurovascular responses, such as functional laser Doppler flowmetry,⁸ fundus photography,⁹ temporal laser speckle imaging,¹⁰ and infrared-differential interference contrast optics.¹¹ However, the common limitation of these technologies is the lack of depth-resolved information, which fails to obtain information in the different layers of retina. Optical coherence tomography (OCT), a noninvasive imaging technique that uses coherent light to capture micrometer-resolution and three-dimensional (3D) images of highly scattering biological tissue, has become a gold standard in ophthalmic imaging in last decade.¹² Moreover, OCT can differentiate individual retinal layers and provide detailed depth-resolved information of the retina by means of high axial resolution. Generally, neural activities can cause morphological changes of cytomembrane as well as cell bodies, further leading to changes of intrinsic optical properties, which are called as intrinsic optical signals (IOSs).¹³ Therefore, OCT provides an excellent technique for depth-resolved IOS recording. Light-evoked IOS changes have already been observed in both photoreceptor layer and inner layers of retina, although the sources of IOSs and mechanisms of mixed polarities are complex and multiple.^{14–16} Meanwhile, Doppler OCT, one of the most principle functional extensions, can provide shifted phase information of backscattered light by Doppler Effect. Additionally, Doppler OCT, capable of detecting retinal vascular responses, has been widely utilized for *in vivo* high-resolution imaging of blood vessels and microvasculature. Several research groups have confirmed that flicker stimulus increases retinal blood flow, which attributes to neurovascular coupling mechanism.^{9,17,18}

Retinal electrostimulation plays a critical role in the neural modulation and visual restoration of ophthalmic diseases and disorders. Noninvasive transcorneal electrical stimulation (TES)¹⁹ has emerged as an evaluation method of residual visual function for patients with severely impaired²⁰ and as a potential therapy to promote retinal cell survival,^{21,22} such as photoreceptors and RGCs, to further facilitate visual restoration and for certain retinal²³ and optic nerve²⁴ disorders at the early or middle stages owing to its neuroprotective effects.^{25–27} In spite of the therapeutic effects have been demonstrated in both animal models and clinical trials,²⁸ it remains largely undefined of the specific therapeutic mechanism of TES and its retinal neurovascular responses. Electroretinogram (ERG), a common technique in electrophysiology of ophthalmology, cannot be used to directly record the retinal activity evoked by electrical currents due to the large artifact from the stimulus.²⁹ By recording electrically evoked potentials in optic chiasma³⁰ and visual cortex,³¹ it was concluded that TES can activate RGCs. Moreover, Fujikado et al. found that TES could activate principally RGCs by fundus camera, and they speculated that TES might induce the neurovascular responses in

the retina and optic nerve as well.^{32,33} Nevertheless, it remains unclarified of the neural activities of other retinal cells and vascular responses evoked by TES due to the lack of depth-resolved information.

Our previous work has already demonstrated that TES could elicit neural responses in all retinal segmented layers.³⁴ Herein, the present study was designed to evaluate neural and vascular responses of retina under TES simultaneously, in order to further investigate neurovascular responses in retina evoked by TES. The study will provide beneficial information on the therapeutic mechanism of TES and a novel technical method to detect retinal neurovascular responses of electrical stimulation.

Materials and methods

Animal preparation

All experimental procedures were strictly performed in accordance with the guidelines of the Care and Use of Laboratory Animals issues by the National Institute of Health and the ethical policies of Shanghai Jiao Tong University.

Four cats (Fengxian, Shanghai, China) with weights of 2.3–2.7 kg were used in this study. After the intramuscular administration of atropine sulfate (0.15 mg/kg; Kelongshouyao, Shanxi, China) to reduce salivation, the cats were initially anesthetized for surgery and OCT recording by intramuscular injection of tiletamine-zolazepam (5 mg/kg; Virbac, Carros, France), followed by artificial ventilation by a pulmonary pump (Model 3000, Matrx, New York, NY, USA) and subsequent anesthesia maintenance by 0.5% isoflurane (RWD Life Science, Shenzhen, Guangdong, China) mixed with air (flow rate 0.8–1.0 mL/min) throughout the experiments. The mixture of gallamine triethiodide (10 mg/kg/h; Sigma-Aldrich, St. Louis, MO, USA) and glucose (24 mg/kg/h; Huayu, Wuxi, Jiangsu, China) was continuously and intravenously infused to maintain the muscle relaxation and nutrition supply. Temperature of cats was kept at approximately 38°C by water-circulating heating pad (T/Pump TP702, Gaymar Industries, New York, NY, USA). Moreover, end tidal carbon dioxide (CO₂), heart rate, and pulse oximetry (SpO₂) were monitored using a multiparameter life monitor (PM-8000 Express, Mindray, Shenzhen, Guangdong, China) throughout the experimental procedure. After preparation, the head of cats were fixed with a stereotaxic frame (SN-3N, Narishige, Tokyo, Japan) with ear and mouth bar to minimize movements caused by breathing and heartbeat. Before the experiments, the pupils were dilated with topical tropicamide (0.5%; Santen Pharmaceutical, Osaka, Japan).

OCT imaging system

The diagram of our custom-designed spectral-domain optical coherence tomography (SD-OCT) system utilized in this study is shown in Figure 1. To be specific, the light source was a near infrared superluminescent diode (SLD, Inphenix, Livermore, CA, USA) with a central wavelength of 840 nm and a bandwidth of 45 nm. A fiber coupler with a splitting ratio of 50:50 divided the light to the sample arm

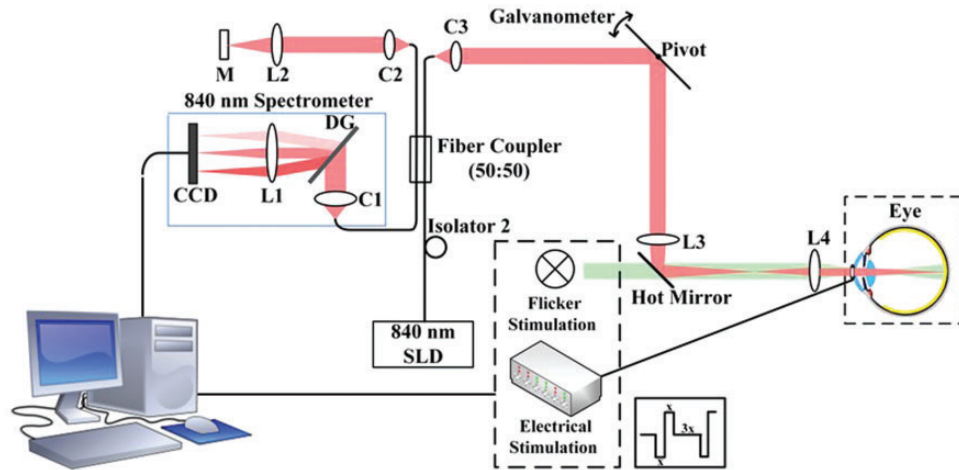


Figure 1. Diagram of the custom-designed SD-OCT system utilized in this study. L1 to L4: lens; C1 to C3: collimating lens; SLD: super luminescent diode; M: mirror; DG: diffraction grating; CCD: charge coupled device. Flicker stimuli and pulse wave electrical stimuli are shown in illustration. (A color version of this figure is available in the online journal.)

and reference arm. A galvanometer (Thorlabs, Newtown, NJ, USA) was utilized to generate 3D OCT images. A linear charge-coupled device camera (Teledyne e2v, Chelmsford, England) with 27 kHz line rate was used to acquire interference signals. The calibrated axial resolution and imaging depth were $7.22 \mu\text{m}$ and 5.16 mm , respectively, in air. The incident power of probe beam at the cornea was set at 0.9 mW , which was safe for eyes according to ANSI Z136.1 (2007). More details about the system were similar and could be found in previous studies.^{35,36}

Retinal stimulation

TES was delivered via a contact lens electrode (ERG-jet, CareFusion, Middleton, WI, USA) placed on the surface of corneal and a return electrode inserted in the neck muscles. Hydroxyethylcellulose gel (1.3%; Santen Pharmaceutical, Osaka, Japan) was applied to protect the cornea and to maintain good conductivity between the electrode and the cornea. Charge-balanced, biphasic, and symmetric rectangular current pulses (cathode-first) of 10 ms pulse width and 20 Hz frequency were generated by an isolated, computer-controlled stimulus generator (STG 4004, Multi-Channel Systems, Reutlingen, Germany) and then synchronized with OCT imaging system. Full-field flicker stimuli (frequency: 20 Hz , pulse width: $10 \mu\text{s}$, illuminance: 45 lux , and 30 s duration) were generated by an isolated flashlamp system (including FD1 Flash Lamp Driver, LS1130 Flashlamp and FO1 Liquid Light Guide, Tucker-Davis Technologies, Alachua, FL, USA), and then entered into the eyes through OCT optical system. In visual stimulation, the tested eye of cats worn a contact lens of appropriate curvature to keep cornea moist. And the fellow eye was covered throughout during the recording procedure. Both TES and flicker stimuli are shown in Figure 1.

Experimental protocol

After fixed on the stereotaxic frame and dark-adapted for 30 min , a 3D retinal imaging was performed using OCT

imaging system. The A-line rate was 27 kHz . And the optic disc was first identified in fundus image of retina, as shown in Figure 2(a). There are three different experiments in this study. In Exp. 1, the simultaneous IOS and vascular changes evoked by TES were investigated. Therefore, blood vessels with high signal-noise rate (SNR) near the optical disc were chosen, and their adjacent areas were applied as the region of interest (ROI). Repeated B-scans with the width of $\sim 0.75 \text{ mm}$ (yellow line in Figure 2(a)) were performed in this region. Each trial was composed of 128 B-scans, and each B-scan contained 512 A-lines, totally lasting for 2.4 s . Five trials were repeated for each stimulation condition with a 3-min trial-to-trial interval for recovery. The data of Exp. 1 derived from five eyes of four cats. In Exp. 2, total vascular responses evoked by TES with prolonged recording time were evaluated. Therefore, the boundary line of a circle with a diameter of 3 mm centered on disc is selected as the ROI, as shown in Figure 2(b). Repeated B-scans with the width of $\sim 9.42 \text{ mm}$ were performed in this region. Each trial contained three scans with 0.8 s scan-to-scan interval due to the restart of the system. And each scan was composed of 8 B-scans and each B-scan consisted of 8192 A-lines, totally lasting for about 9 s . Five trials were repeated for each stimulation condition with 5-min trail-to-trail interval for recovery. The data of Exp. 2 derived from four eyes of three cats. Various current intensities ($0, 1.0, 2.0, \text{ and } 3.0 \text{ mA}$) with the duration of 1 s were applied in both Exp. 1 and 2. In Exp. 3, vascular changes evoked by light stimuli were examined. The protocol turned out to be almost same with that of Exp. 1, but was different in stimuli and recording time. Flicker stimulation time was prolonged to 30 s and recording time was set as approximately 38 s . Thus, each trial consisted of 12 scans with 0.8 s scan-to-scan interval. The data of Exp.3 were derived from four eyes of three cats.

IOS data processing

The IOS changes are defined as the stimulus-evoked changes of intrinsic optical properties, which mainly

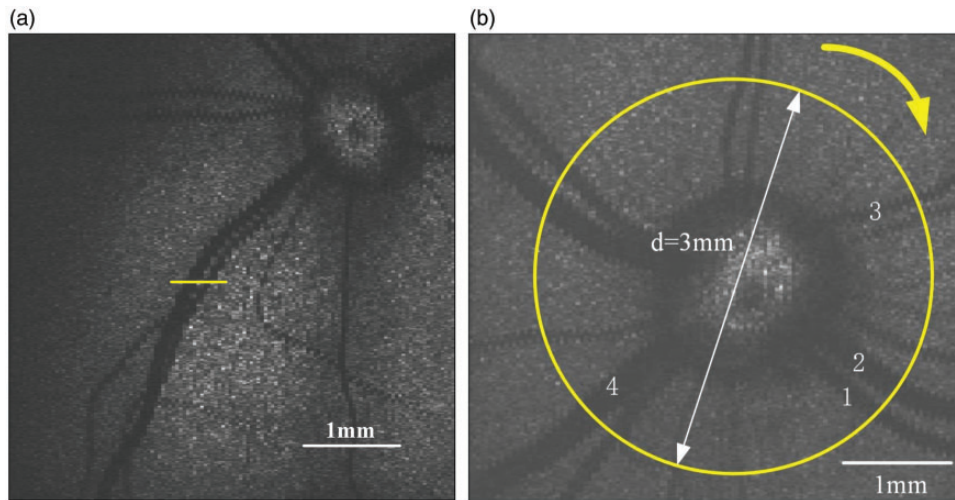


Figure 2. Typical fundus image of retina by SD-OCT and different retinal scanning protocols for cats. (a) Line scanning position. (b) Circular scanning position. Yellow lines represent the locations where OCT probe beam scanned in both pictures. (A color version of this figure is available in the online journal.)

reflects light scattering in our study. They can be expressed as $\Delta I/I$, where ΔI indicates the stimulus-evoked magnitude change and I suggests the magnitude before the stimulation.¹⁴ Data analysis was performed on MATLAB (MathWorks, Natick, MA, USA) using user-defined programs. Firstly, the acquired B-scan images in a trial were registered using MATLAB function *imregister*. The first B-scan image of each trail was used as the reference for registering the subsequent images. As the B-scan images were realized by bidirectional raster scanning, the images corresponding to opposite scan directions might be laterally misaligned due to limited precision of the galvanometer system, whereas the image registration method could not totally eliminate this misalignment. Hence, only half of the B-scan images corresponding to the same scan direction were used for the following data analysis in each trail. In order to evaluate the IOS changes in different layers, the retina was segmented into three parts in depth: inner retina from inner limiting membrane to outer plexiform layer (OPL), outer retina from OPL to the junction between inner segment of photoreceptor and outer segment of photoreceptor (IS/OS), and subretinal space from IS/OS to retinal pigment epithelium (RPE)-Bruch's membrane, which was applied by an open source toolbox of OCT retinal segmentation in MATLAB.³⁴ For each trail, the differential images ΔI were obtained by subtracting the reference image I , which is the mean intensity of OCT signals averaged from the first four images, from all the remaining images in the trail. To increase the SNR, the final ΔI were averaged by two consecutive ΔI . Therefore, the frame rate of the ΔI was one-quarter of B-scan rate. To obtain fractional IOS changes, ΔI was divided by the I on a pixel-to-pixel basis. In order to attenuate the influence of fluctuation and to intuitively reveal the changes, 0.7 and -0.5 were chosen as the threshold values for positive and negative IOSs, respectively, according to our preliminary experiments. Therefore, in this study, the pixels satisfying $\Delta I/I > 0.7$ were defined as positive pixels, while

the pixels satisfying $\Delta I/I < -0.5$ were defined as negative pixels. For quantitative evaluation of the IOS changes, two parameters about the IOSs were further defined: the ratio of positive/negative pixels in each part, namely $Ratio^+$ and $Ratio^-$, which was calculated by the ratio of the number of positive/negative pixels and the number of all pixels in each part. To investigate the simultaneous neural and vascular responses, scanning positions were chosen at locations containing vessels in the retina and IOS changes were extracted from the area adjacent to the vessels.

Doppler OCT data processing

Doppler OCT is able to extract phase shifts in the backscattered light, which could, therefore, provide information on particle movements in the probed tissue region.⁹ The flow velocity of fluid can be calculated by Doppler principle using the following formula

$$v = \frac{\lambda \Delta \Phi}{4\pi n \tau \cos \alpha}$$

where λ is the central wavelength of the light source and $\Delta \Phi$ is the phase difference between subsequent A-lines, n represents the index of refraction and τ represents the time interval between subsequent A-lines. α in equation above is the Doppler angle between probe beam and particle movement.

The unambiguous phase difference calculated via Fourier transform was within the range $[-\pi, \pi]$. However, in the case of quite high-flow velocities, the phase difference can exceed this range, called phase wrapping, which could be achieved by adding or subtracting 2π to a phase corresponding to the flow. Bulk motion algorithm based on histogram analysis³⁷ was also applied to get accurate phase fluctuations. The vessels measured in this study were approximately 2 mm to the optic nerve head (ONH) and obtained a wider range of measured velocity. Both phase

unwrapping and bulk motion compensation were performed in the Doppler OCT images to obtain accurate blood flow inside the vessels. In addition, the Doppler angle was carefully maintained constant throughout the experiments. Therefore, the phase difference inside the vessel was proportional to the blood velocity and the phase difference alone could be used to represent the blood velocity.

Doppler OCT phantom experiment

Before *in vivo* experiments, phantom assays were performed to measure the accuracy, range, and precision of the Doppler method in our SD-OCT system. Dilute milk (50%) in the microtube (94-2702, SANSYO, Tokyo, Japan) with an inner diameter of 0.5 mm was driven by a peristaltic pump (BT100-2J, LongerPump, Baoding, Hebei, China) at preset flow velocity. Lens L4 (Figure 1) was taken down for focusing on the microtube by the probe beam. Afterwards, measured velocity was calculated by equation above. As shown in Figure 3, the measured velocity was almost equal to the preset velocity in the range of 4 mm/s to 17 mm/s, further demonstrating the feasibility of our method.

Results

IOS changes

The fundus image of retina and segmentation of retinal layers post-processed from OCT data are shown in Figures 2(b) and 4. IOSs were extracted and analyzed in the following three segment parts: inner retina, outer retina, and subretinal space. To investigate the depth-resolved characteristics of TES-induced IOSs in retina, data averaged across five eyes from four cats were analyzed to present a statistical illustration in Figure 5, where yellow rectangles indicated 1 s stimulation duration.

The time course of $Ratio^+$ and $Ratio^-$ in the inner retina are displayed in Figure 5(a) and (b), respectively. Physiologically, the inner retina includes RGCs and their nerve fibers, bipolar cells as well as synaptic junctions between RGCs and bipolar cells. Both $Ratio^+$ and $Ratio^-$ increased significantly after the application of TES. These changes lasted during the stimulation and decreased after the cessation of TES. The increased amplitudes of $Ratio^+$ and $Ratio^-$ were almost equal in each group. Besides, these changes increased more significantly with higher applied current intensity. Therefore, the increases of $Ratio^+$ and $Ratio^-$ were highly associated with TES, indicating that TES could induce the increase of $Ratio^+$ and $Ratio^-$.

Figure 5(c) and (d) displays the changes of $Ratio^+$ and $Ratio^-$ in the outer retina, which includes photoreceptor cell bodies and inner segments. Similar to the changes in the inner retina, TES has been observed to be able to induce the increase of $Ratio^+$ and $Ratio^-$ in this part as well. But the increased amplitudes of $Ratio^-$ were much higher than that of $Ratio^+$, comparing with those almost equal in the inner retina. Moreover, the increased magnitudes were higher in each group of same TES intensity in comparison with the inner retina.

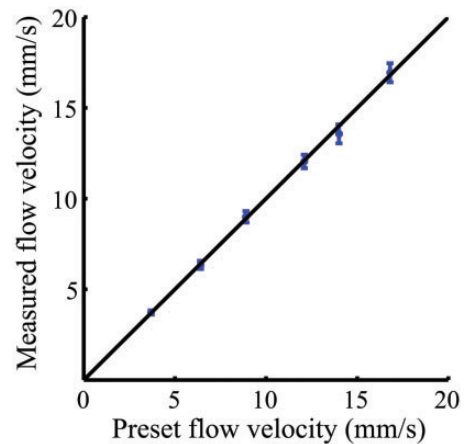


Figure 3. Relationship between the preset velocity and measured flow velocity by phase-resolved SD-OCT in microtube. (A color version of this figure is available in the online journal.)

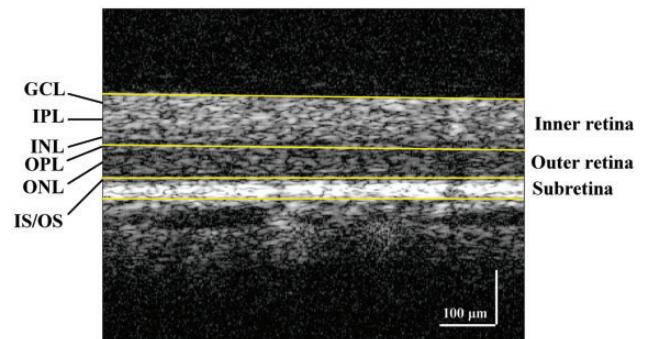


Figure 4. Retinal segmentation layers for cats. ILM: inner limiting membrane; GCL: ganglion cell layer; IPL: inner plexiform layer; INL: inner nuclear layer; OPL: outer plexiform layer; ONL: outer nuclear layer; IS/OS: the junction between inner segments of photoreceptor and outer segments of photoreceptor; RPE: retinal pigment epithelium. (A color version of this figure is available in the online journal.)

The changes of $Ratio^+$ and $Ratio^-$ in the subretinal space, which includes the outer segment of photoreceptors, RPE cells, and a part of tapetum, are shown in Figure 5(e) and (f). Consistent to the first two parts, $Ratio^+$ and $Ratio^-$ increased with TES. However, in the opposite of those in the outer retina, the increased magnitudes of $Ratio^-$ were weaker than those of $Ratio^+$. Of note, the increased magnitudes in the subretinal space were the highest in all three parts.

Slow increases were also observed in the control groups, which could attribute to intrinsic noises and mechanical error of galvanometer during scanning. In addition, the recording time after stimulation was only 0.8 s, which was not long enough to explore the total time course of IOS changes.

Vascular changes

To investigate the possible coinstantaneous neural and vascular responses with IOSs at the same location during the application of TES, we selected the area containing blood vessels with high SNR near the optical disc and their

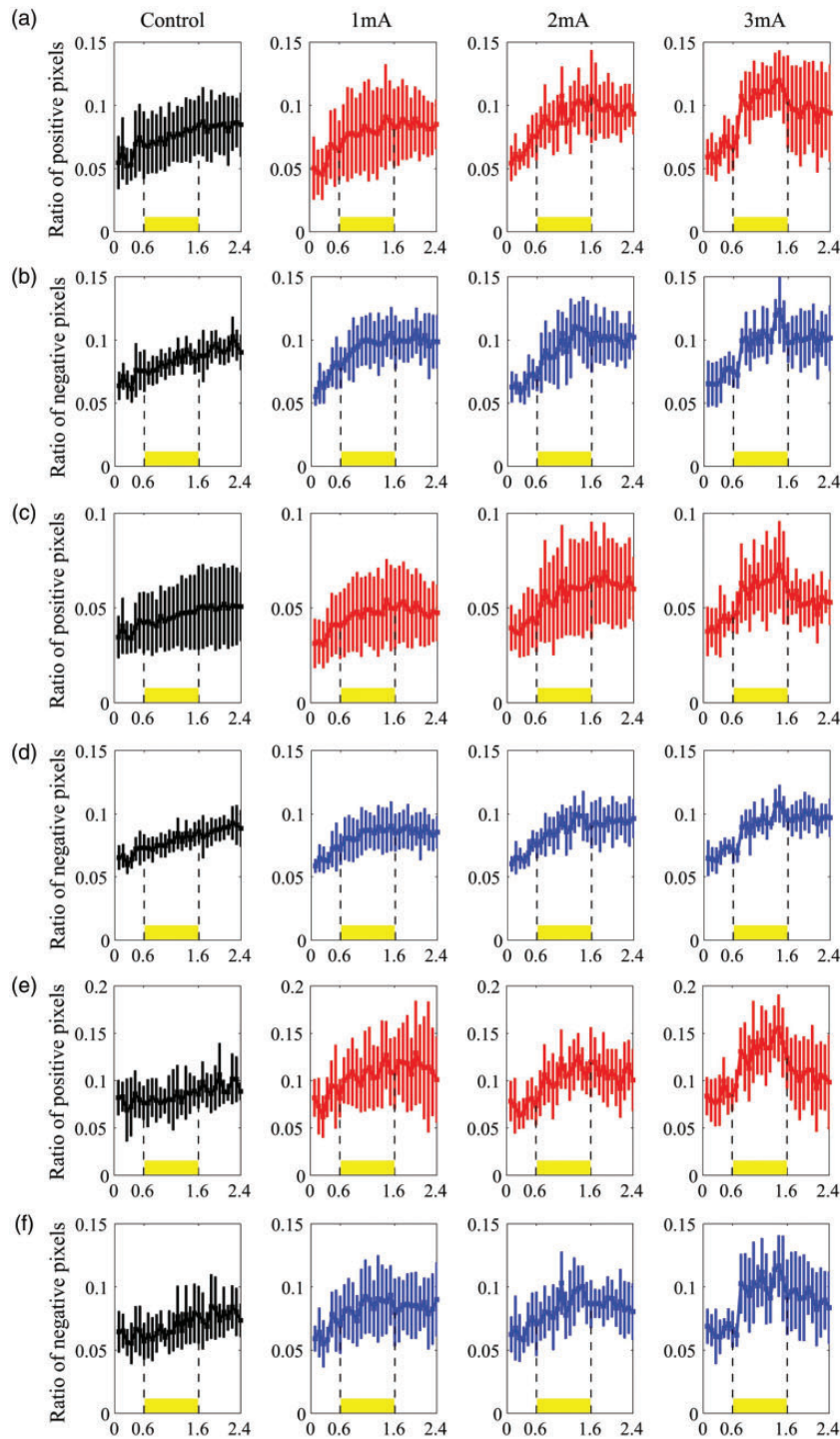


Figure 5. The time course of the ratios of positive and negative pixels of IOS changes in segmented layers under TES with various current intensities: (a–b) inner retina, (c–d) outer retina, and (e–f) subretinal space. The yellow rectangles represent stimulation duration for 1 s. (A color version of this figure is available in the online journal.)

adjacent areas as the ROI. Figure 6(a) represents the Doppler OCT imaging of ROI. There are two blood vessels in the figure. Concisely, the right side is an artery and the left side is a vein. Because the flow directions of the retinal artery and vein are opposite (the artery flows out of the optic disc, while the vein flows into the optic disc), the extracted phase difference according to the Doppler frequency shift is also distinct. In addition, the arterial changes were more pronounced during the stimulation.

Thus, the artery was selected for subsequent process and analysis. The pulsatile phase was extracted from OCT data recording during *in vivo* experiments. As shown in Figure 6 (b), the pulsatile frequency was in accordance with the frequency of heartbeats, indicating the high accuracy of our method. To evaluate the retinal vascular responses under TES, we extracted the change rates of blood velocity, cross-sectional area of vessel, and blood flow from Doppler OCT images. The results of single retinal vascular responses

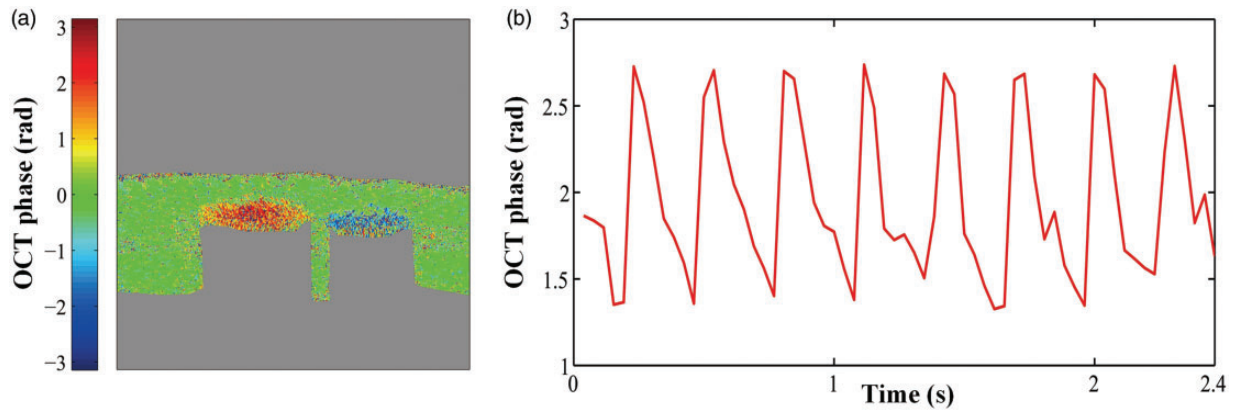


Figure 6. Doppler OCT imaging *in vivo*. (a) Typical Doppler OCT image of retinal vessels by line scanning. (b) Phase variation with time inside the artery extracted from OCT data. (A color version of this figure is available in the online journal.)

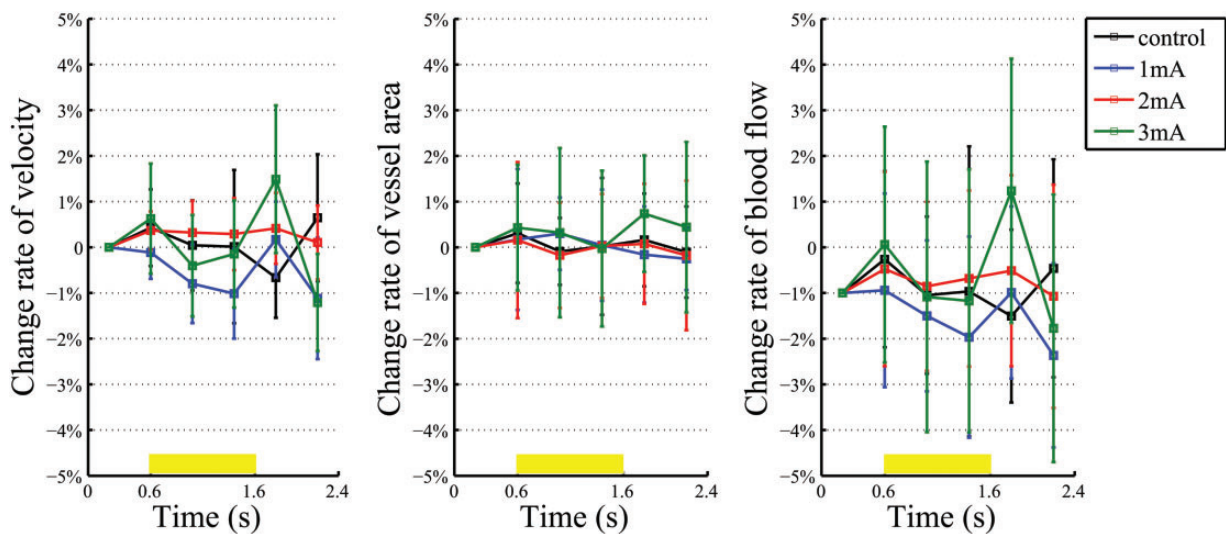


Figure 7. Change rate of (a) blood velocity, (b) cross-sectional area of vessel, and (c) blood flow of retina under TES (from response of single major retinal vessel in each experiment). The yellow rectangles represent stimulation period. Data above are presented as means \pm SD. (A color version of this figure is available in the online journal.)

under TES are shown in Figure 7. The parameters of vessels were calculated in several heartbeat cycles. The changes before, during, and after TES were not obvious. The changes of vascular responses were all within the range of $\pm 3\%$, which were in the error range due to the noise. In addition, based on t-test, there was showed no significant difference between experimental groups and the control groups, which was suggestive of the unobvious changes of retinal vascular responses under TES.

To investigate the total vascular responses in retina under TES, circular scanning was used (Figure 2(b)). Similar to the aforementioned reason, main arteries were chosen for data processing and analysis as the red division shown in Figure 8. As shown in Figure 9, the sum responses of several major vascular were within approximately 9 s. Similar to the above results, the changes of vascular responses were all in the range of $\pm 5\%$, which also reveals the unobvious changes of retinal vascular responses under TES.

The changes of velocity in retinal vessels under 30 s flicker stimulation were also measured. The change rate of

velocity in retinal vessels under 30 s flicker stimulation is shown in Figure 10. As a result, the velocity increased slowly during the stimulation and reached about an increase rate of 8% at the end of stimulation, illustrating that flicker stimulation can increase retinal blood flow.

Discussion

In the present study, we demonstrated that TES could evoke IOS changes in all three segmented retinal layers of cats, whereas the retinal vascular responses evoked by TES were almost unchanged with three different experimental protocols.

Experimental protocols

Doppler OCT can obtain the distribution of the object motion velocity by calculating the phase differences between two adjacent A-lines.³⁸ There were 1.5 μm apart on the retina to guarantee that the distance between A-lines is much smaller than the optical spot size in our system. Moreover, the limitation of data capacity was

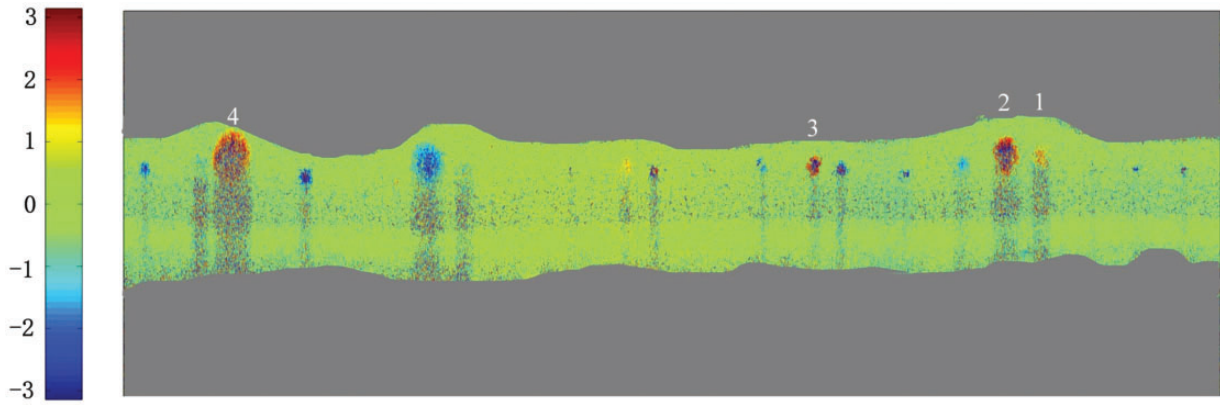


Figure 8. Typical Doppler OCT image of total retinal vessels by circular scanning. (A color version of this figure is available in the online journal.)

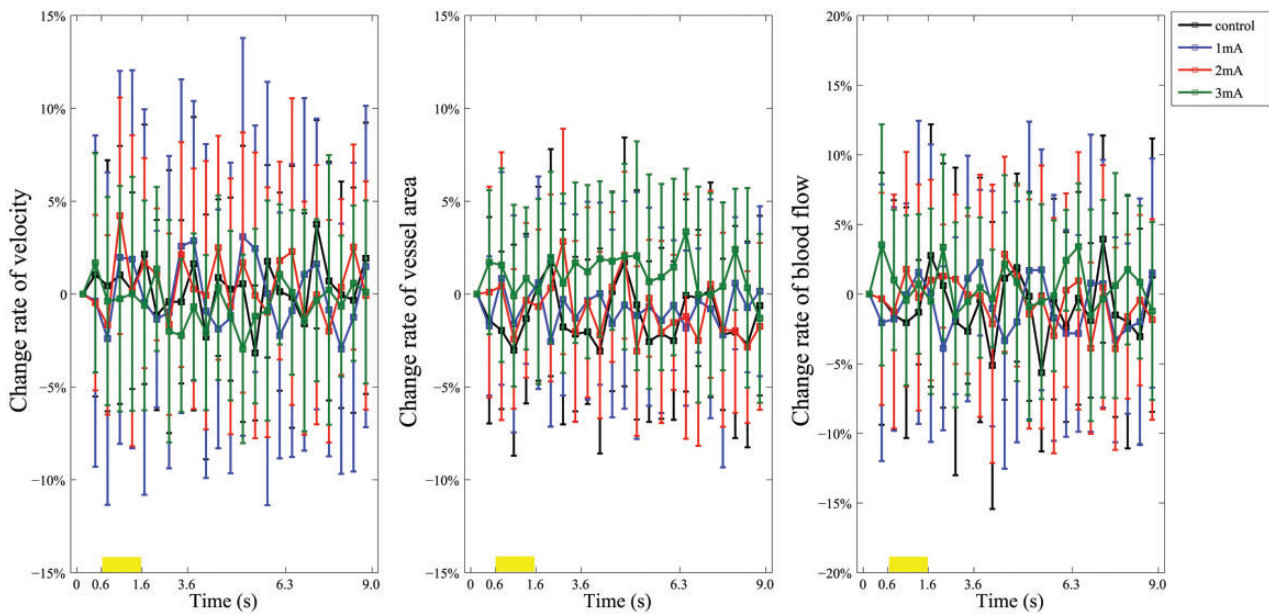


Figure 9. Change rate of (a) blood velocity, (b) cross-sectional area of vessel, and (c) blood flow of retina under TES (from sum responses of several major retinal vessels in each experiment). The yellow rectangles represent stimulation period. Data above are presented as means \pm SD. (A color version of this figure is available in the online journal.)

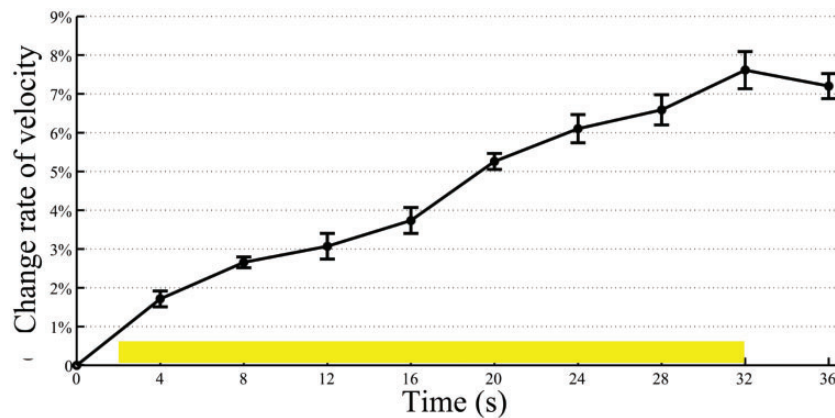


Figure 10. The change rate of velocity in retinal vessels under 30 s-flicker stimulation. The yellow rectangle represents stimulation period. Data above are presented as means \pm SD. (A color version of this figure is available in the online journal.)

65,536 A-lines. Thus, different experimental protocols for different experiments were designed. In Exp. 1, the width of ~ 0.75 mm (Figure 2(a)) with a high temporal resolution (~ 19 ms, 512 A-lines*128 B-scans) was scanned to record simultaneous neural and vascular responses for 2.4 s in each trail. Different neural responses were detected under TES with various parameters, while the responses of single retinal vascular were not significant. However, there were certain deficiencies in Exp. 1. On one hand, scanning position only included single major retinal vessel in each experiment, which cannot reflect the total vascular responses of the retina. On the other hand, vascular responses may be delayed, while 0.8 s post-stimulus period was not long enough to record the delayed responses. To overcome the deficiencies, circular scanning for ~ 9.4 mm was used to obtain total vascular responses (Figure 2(b)). In order to meet requirements of the spatial resolution for Doppler OCT, 8192 A-lines*8 B-scans mode was selected by sacrificing the temporal resolution (0.3 s). In addition, the number of scanning was also three times to ~ 9 s in order to record the possible delayed responses. The results still revealed unobvious changes in retinal vascular responses under TES. To verify the reliability of our results, the changes in velocity in retinal vessels were also measured under 30 s flicker stimuli. The results showed that during the flicker stimulation, significant vascular responses kept increasing, which was consistent with the results proven in previous reports.^{9,17,18} This conclusion firmly verified the reliability of the OCT system and experimental animals, and further proved the validity of the responses evoked by TES.

Neural responses

Our results showed significant IOS changes could be evoked by TES in all three segmented retinal layers, which were positively correlated with the stimulation current intensity. It is consistent with the results in the study of Morimoto et al., revealing that the intensities of reflectance changes (RCs) were dependent on the stimulus parameters of TES.³³ In other words, scattering changes could be evoked by TES in the whole retina during the stimulation. In addition, both positive and negative scattering changes were detected, while the magnitude of TES-induced IOSs was the strongest in the subretinal space and the lowest in the inner retina. The magnitudes of IOSs changes were surprisingly in accordance with the results under light stimulation,^{13,15,39} which could also be detected in all retinal layers.^{13,40} The possible reasons for these light-induced changes are the binding and release of G-proteins as well as photoexcited rhodopsin, localized biochemical processes, and photoreceptor outer segment disk swelling/shrinkage.¹⁴ However, in the present study, several possible effects may account for TES-induced scattering changes, including the retinal neural responses evoked by TES, and other factors unrelated to cellular neural activity, for instance, noise artifacts generated by optical imaging system during recording and hemodynamic responses as well as retinal structural and morphological changes caused by extrinsic electrical stimulation.

Plenty of researches have already demonstrated that TES could effectively activate neurons in retina.^{29–32} However, the specific acting site varies from study to study due to the different recording and analyzing methods. Initial studies have suggested that TES could activate the inner retina, which is the mainstream view to date.^{30–32} Morimoto et al. have revealed that retinal reflectance changes (RCs) represented the response of neural activity and TES might stimulate RGCs and optic nerve; therefore, neural activities of retina could induce the scattering changes.³³ Moreover, our previous study has also discussed the possibility that TES might activate the outer retina.³⁴ Although the activated TES-evoked retinal layers should be further investigated using methods with higher spatial and depth resolution, there is no doubt that scattering changes are related with the retinal neural responses.

In addition, hemodynamic responses may cause the scattering changes of retina.^{32,33} However, the area where IOSs extracted from did not contain any retinal vessels, demonstrating that hemodynamic responses could not be the possible reason for scattering changes in this study. Generally, there is a delay of 2–3 s in the scattering changes caused by hemodynamic responses,³² while the observed scattering changes started within 75.8 ms, which is the time resolution of our devices. On the other hand, in our study, we did not observe any significant vascular changes evoked by TES. Combined with the above points, we suggest that hemodynamic responses are independent from the scattering changes caused by TES.

Inomata et al. reported that TES with intensity higher than 1 mA would cause a degradation in the imaging quality with mosaic imaging artifacts induced by recording changes in the reflectance of infrared light from the monkey retinas after transscleral electrical stimulation by DTL electrodes.²⁹ They suggested that the degraded imaging quality was caused by the vibration of corneal epithelium and the constriction of choroidal arterial. Additionally, the distortions and thickness changes of retina may also result in imaging artifacts. To exclude these possible causes, our previous work has demonstrated that TES within 3.0 mA would not cause image quality degradation without discernible mosaic imaging artifacts or detectable distortion or thickness changes of retina.³⁴ And results conflicted with aforementioned studies may be due to the different stimulating electrodes and recording methods.

In conclusion, we suggest that the TES-induced scattering changes of retina are partly related to the retinal cellular neural responses, although further investigations are warranted to explore the underlying physiological mechanisms and specific activated cell types.

Vascular responses

We also detected retinal vascular responses under TES. We measured the blood velocity, cross-sectional area of vessel and blood flow of both single retinal vessel and several major retinal vessels evoked by TES. Different from neural responses, there were no significant changes before, during, and after electrical stimulation, which is

totally different with the results under visual stimulation as well. David group investigated that the blood flow, arterial vessel cross-sectional area, and arterial flow velocity increased 22.2%, 2.7%, and 18.3%, respectively, after 30 s of flicker stimulation in human eyes with Doppler Fourier-domain OCT (FD-OCT).¹⁷ Werkmeister et al. investigated that the retinal vessel diameter, blood velocity, and blood flow increased 3.4%, 28.1%, and 36.2%, respectively, after 60 s of diffuse flicker stimulation in rat eyes with combination of Doppler FD-OCT and fundus camera.⁹ Our experiment also reported that the velocity of retinal vessels increased 8% after 30 s flicker stimulation, which verified the reliability of the system. The smaller change may be due to the shorter pulse width of light stimuli, only 10 μ s, which is almost thousandth of the other studies. However, we did not observe significant vascular changes during TES experiments, which might be the result from different processing pathways between visual and electrical stimulation. There was also the possibility that the responses evoked by our electrical stimuli protocol were extremely small. Therefore, the changes may be drowned by the noise, or may only exist in capillaries as well.

Different processing pathways with different intrinsic processing mechanism between visual as well as electrical stimulation may be the explanation for various vascular responses. In normal vision, photoreceptors convert light into electrical signals to stimulate subsequent biological processes, which is called phototransduction. However, as manifested by the aforementioned results, TES mainly activated inner retina neurons (primarily RGCs) instead of photoreceptors.^{30,41} Besides, there are about 96.6 million photoreceptors in the human retina,⁴² while only about 0.7 to 1.5 million RCCs per retina.⁴³ The lack of phototransduction, light adaption, and fewer neurons involved in TES would significantly reduce energy consumption.⁴⁴ And the retinal vascular system provides a sufficient energy source for retina. Thus, the lack of energy-consuming process may dramatically reduce vascular responses under TES compared to significant vascular changes under light stimulation.

However, there was also the possibility that the responses evoked by our electrical stimuli protocol were extremely small. Fujikado group explored the changes of RCs evoked by TES using different parameters by fundus camera.³³ They found that amplitudes of responses under 4 s-TES were five times greater than those under 1 s-TES. We cautiously speculate that vascular responses were extremely sensitive to change of stimulus duration. Thus, the responses evoked by 1 s-stimuli were too small to be covered by the noise. However, previous research revealed that current intensity more than 3.6 mA would evoke abrupt change in cortical responses of cats.⁴⁵ Thus, we did not prolong our stimuli protocol with maximum intensity of 3.0 mA in consideration of safety factors. In addition, charge deliver efficiency varies between different electrodes could result in inconsistent results as well. Moreover, Kurimoto et al. found that prolonged TES for 3 and 24 h would significantly increase chorioretinal blood flow in normal human subjects.⁴⁶ Thus, the 1 s-stimuli might only evoked responses in choroid capillary. However, we only

measure the major retinal arteries around the ONH with the limited resolution devices. The vascular changes evoked by our stimuli protocol might be extremely small, resulting in the changes drowned by the noise. There was also the possibility that these small changes only existed in capillaries. Thus, the recording of changes in retinal vessels was not obvious.

To sum up, vascular responses evoked by TES were almost unvaried in present study, which was quite different from those evoked by light stimuli. These phenomena may be mainly caused by different processing pathways between visual and electrical stimulation. Additionally, small TES-evoked responses might be another explanation.

In summary, we explored the retinal neural and vascular responses under TES simultaneously with custom-designed SD-OCT. Both positive and negative IOS changes could be evoked in three segmented parts in retina. And to rule out other possible factors, we suggested that these scattering changes were mainly related to the retinal neural responses. Vascular responses were not significant in the present. Different processing pathways with different intrinsic processing mechanisms between visual and electrical stimulation may result in these various vascular responses. Small TES-evoked responses may be another explanation. Thus, we concluded that TES predominately evoked neural responses in retina, while vascular responses were not obvious. These results provide beneficial references to the mechanism of retinal neurovascular coupling under TES. And the present study suggests that SD-OCT could be utilized as a novel method in clinical treatment as well as technology to detect neurovascular responses with retinal stimulation. Nevertheless, further studies are necessary to obtain more comprehensive understandings of neurovascular responses and their mechanism evoked by TES with higher spatiotemporal resolution devices.

Authors' contributions: XS, HZ, QL, and CZ designed the experiment; XS, HZ, and PS conducted the experiment; HZ analyzed the data; XS and CZ wrote the manuscript; MZ, HL, JG, and XC participated in discussion. All authors reviewed the manuscript. XS and HZ contributed equally to this work.


DECLARATION OF CONFLICTING INTERESTS

The authors declare no conflict of interest with respect to the research, authorship, and/or publication of this article.

FUNDING

The author(s) disclosed receipt of the following financial support for the research, authorship, and/or publication of this article: This work was supported by the National Natural Science Foundation of China (grant numbers 62875123 and 61773256), the Science and Technology Commission of Shanghai Municipality (grant numbers 17441902900), the Medical-Engineering Cross Foundation of Shanghai Jiao Tong University (grant number YG2016ZD07), and the Project funded by China Postdoctoral Science Foundation (grant number 2019M661509).

ORCID iD

Chuanqing Zhou  <https://orcid.org/0000-0002-1368-7222>

REFERENCES

- Roy CS, Sherrington CS. On the regulation of the blood-supply of the brain. *J Physiol (Lond)* 1890;**11**:85–158
- Riva CE, Logean E, Falsini B. Visually evoked hemodynamical response and assessment of neurovascular coupling in the optic nerve and retina. *Prog Retin Eye Res* 2005;**24**:183–215
- Wassle H, Boycott BB. Functional architecture of the mammalian retina. *Physiol Rev* 1991;**71**:447–80
- Pemp B, Schmetterer L. Ocular blood flow in diabetes and age-related macular degeneration. *Can J Ophthalmol* 2008;**43**:295–301
- Told R, Palkovits S, Boltz A, Schmidl D, Napora KJ, Werkmeister RM, Haslachner H, Frantal S, Popa Cherecheanu A, Schmetterer L. Flicker-induced retinal vasodilatation is not dependent on complement factor H polymorphism in healthy young subjects. *Acta Ophthalmologica* 2014;**92**:e540–5
- Kanda H, Mihashi T, Miyoshi T, Hirohara Y, Morimoto T, Terasawa Y, Fujikado T. Evaluation of electrochemically treated bulk electrodes for a retinal prosthesis by examination of retinal intrinsic signals in cats. *Jpn J Ophthalmol* 2014;**58**:309–19
- Cherecheanu AP, Garhofer G, Schmidl D, Werkmeister R, Schmetterer L. Ocular perfusion pressure and ocular blood flow in glaucoma. *Curr Opin Pharmacol* 2013;**13**:36–42
- Riva CE, Falsini B. Functional laser Doppler flowmetry of the optic nerve: physiological aspects and clinical applications. *Prog Brain Res* 2008;**173**:149–63
- Werkmeister RM, Vietauer M, Knopf C, Fürnsinn C, Leitgeb RA, Reitsamer H, Gröschl M, Garhöfer G, Vilser W, Schmetterer L. Measurement of retinal blood flow in the rat by combining Doppler Fourier-domain optical coherence tomography with fundus imaging. *J Biomed Opt* 2014;**19**:106008
- Li N, Jia X, Murari K, Parlapalli R, Rege A, Thakor NV. High spatiotemporal resolution imaging of the neurovascular response to electrical stimulation of rat peripheral trigeminal nerve as revealed by in vivo temporal laser speckle contrast. *J Neurosci Methods* 2009;**176**:230–6
- Metaea MR, Newman EA. Glial cells dilate and constrict blood vessels: a mechanism of neurovascular coupling. *J Neurosci* 2006;**26**:2862–70
- Huang D, Swanson EA, Lin CP, Schuman JS, Stinson WG, Chang W, Hee MR, Flotte T, Gregory K, Puliafito CA. Optical coherence tomography. *Science* 1991;**254**:1178–81
- Bizheva K, Pflug R, Hermann B, Považay B, Sattmann H, Qiu P, Anger E, Reitsamer H, Popov S, Taylor JR. Optophysiology: depth-resolved probing of retinal physiology with functional ultrahigh-resolution optical coherence tomography. *Proc Natl Acad Sci USA* 2006;**103**:5066–71
- Yao X, Wang B. Intrinsic optical signal imaging of retinal physiology: a review. *J Biomed Opt* 2015;**20**:090901
- Zhang Q, Lu R, Wang B, Messinger JD, Curcio CA, Yao X. Functional optical coherence tomography enables in vivo physiological assessment of retinal rod and cone photoreceptors. *Sci Rep* 2015;**5**:9595
- Son T, Wang B, Thapa D, Lu Y, Chen Y, Cao D, Yao X. Optical coherence tomography angiography of stimulus evoked hemodynamic responses in individual retinal layers. *Biomed Opt Express* 2016;**7**:3151–62
- Wang Y, Fawzi AA, Tan O, Zhang X, Huang D. Flicker-induced changes in retinal blood flow assessed by doppler optical coherence tomography. *Biomed Opt Express* 2011;**2**:1852–60
- Tan B, Mason E, MacLellan B, Bizheva KK. Correlation of visually evoked functional and blood flow changes in the rat retina measured with a combined OCT+ ERG system. *Invest Ophthalmol Vis Sci* 2017;**58**:1673–81
- Fu L, Lo ACY, Lai JSM, Shih KC. The role of electrical stimulation therapy in ophthalmic diseases. *Graefes Arch Clin Exp Ophthalmol* 2015;**253**:171–6
- Morimoto T, Fukui T, Matsushita K, Okawa Y, Shimojyo H, Kusaka S, Tano Y, Fujikado T. Evaluation of residual retinal function by pupillary constrictions and phosphenes using transcorneal electrical stimulation in patients with retinal degeneration. *Graefes Arch Clin Exp Ophthalmol* 2006;**244**:1283–92
- Morimoto T, Fujikado T, Choi J-S, Kanda H, Miyoshi T, Fukuda Y, Tano Y. Transcorneal electrical stimulation promotes the survival of photoreceptors and preserves retinal function in royal college of surgeons rats. *Invest Ophthalmol Vis Sci* 2007;**48**:4725–32
- Henrich-Noack P, Voigt N, Prilloff S, Fedorov A, Sabel BA. Transcorneal electrical stimulation alters morphology and survival of retinal ganglion cells after optic nerve damage. *Neurosci Lett* 2013;**543**:1–6
- Schatz A, Pach J, Gosheva M, Naycheva L, Willmann G, Wilhelm B, Peters T, Bartz-Schmidt KU, Zrenner E, Messias A. Transcorneal electrical stimulation for patients with retinitis pigmentosa: a prospective, randomized, sham-controlled follow-up study over 1 year. *Invest Ophthalmol Vis Sci* 2017;**58**:257–69
- Fedorov A, Jobke S, Bersnev V, Chibisova A, Chibisova Y, Gall C, Sabel BA. Restoration of vision after optic nerve lesions with noninvasive transorbital alternating current stimulation: a clinical observational study. *Brain Stimul* 2011;**4**:189–201
- Ni Y-Q, Gan D-K, Xu H-D, Xu G-Z. Neuroprotective effect of transcorneal electrical stimulation on light-induced photoreceptor degeneration. *Exp Neurol* 2009;**219**:439–52
- Wang X, Mo X, Li D, Wang Y, Fang Y, Rong X, Miao H, Shou T. Neuroprotective effect of transcorneal electrical stimulation on ischemic damage in the rat retina. *Exp Eye Res* 2011;**93**:753–60
- Morimoto T, Miyoshi T, Sawai H, Fujikado T. Optimal parameters of transcorneal electrical stimulation (TES) to be neuroprotective of axotomized RGCs in adult rats. *Exp Eye Res* 2010;**90**:285–91
- Tao Y, Chen T, Liu B, Wang L-Q, Peng G-H, Qin L-M, Yan Z-J, Huang Y-F. The transcorneal electrical stimulation as a novel therapeutic strategy against retinal and optic neuropathy: a review of experimental and clinical trials. *Int J Ophthalmol* 2016;**9**:914–9
- Inomata K, Tsunoda K, Hanazono G, Kazato Y, Shinoda K, Yuzawa M, Tanifuji M, Miyake Y. Distribution of retinal responses evoked by transscleral electrical stimulation detected by intrinsic signal imaging in macaque monkeys. *Invest Ophthalmol Vis Sci* 2008;**49**:2193–200
- Shimazu K, Miyake Y, Watanabe S. Retinal ganglion cell response properties in the transcorneal electrically evoked response of the visual system. *Vision Res* 1999;**39**:2251–60
- Foik AT, Kublik E, Sergeeva EG, Tatlisumak T, Rossini PM, Sabel BA, Waleszczyk WJ. Retinal origin of electrically evoked potentials in response to transcorneal alternating current stimulation in the rat. *Invest Ophthalmol Vis Sci* 2015;**56**:1711–8
- Mihashi T, Okawa Y, Miyoshi T, Kitaguchi Y, Hirohara Y, Fujikado T. Comparing retinal reflectance changes elicited by transcorneal electrical retinal stimulation with those of optic chiasma stimulation in cats. *Jpn J Ophthalmol* 2011;**55**:49–56
- Morimoto T, Kanda H, Miyoshi T, Hirohara Y, Mihashi T, Kitaguchi Y, Nishida K, Fujikado T. Characteristics of retinal reflectance changes induced by transcorneal electrical stimulation in cat eyes. *PLoS One* 2014;**9**:e92186
- Sun P, Li Q, Li H, Di L, Su X, Chen J, Zheng H, Chen Y, Zhou C, Chai X. Depth-Resolved physiological response of retina to transcorneal electrical stimulation measured with optical coherence tomography. *IEEE Trans Neural Syst Rehabil Eng* 2019;**27**:905–15
- Fan S, Li L, Li Q, Dai C, Ren Q, Jiao S, Zhou C. Dual band dual focus optical coherence tomography for imaging the whole eye segment. *Biomed Opt Express* 2015;**6**:2481–93
- Li Q, Li L, Fan S, Dai C, Chai X, Zhou C. Retinal pulse wave velocity measurement using spectral-domain optical coherence tomography. *J Biophotonics* 2018;**11**:e201700163
- Kolbitsch C, Schmoll T, Leitgeb RA. Histogram-based filtering for quantitative 3D retinal angiography. *J Biophotonics* 2009;**2**:416–25
- Drexler W, Fujimoto JG. *Optical coherence tomography: technology and applications*. Berlin: Springer Science & Business Media, 2008.

39. Wang B, Lu Y, Yao X. In vivo optical coherence tomography of stimulus-evoked intrinsic optical signals in mouse retinas. *J Biomed Opt* 2016;**21**:096010
40. Moayed AA, Hariri S, Choh V, Bizheva K. In vivo imaging of intrinsic optical signals in chicken retina with functional optical coherence tomography. *Opt Lett* 2011;**36**:4575-7
41. Potts AM, Inoue J. The electrically evoked response of the visual system (EER): III. Further contribution to the origin of the EER. *Invest Ophthalmol Vis Sci* 1970;**9**:814-9
42. Curcio CA, Sloan KR, Kalina RE, Hendrickson AE. Human photoreceptor topography. *J Comp Neurol* 1990;**292**:497-523
43. Watson AB. A formula for human retinal ganglion cell receptive field density as a function of visual field location. *J Vis* 2014;**14**:15
44. Okawa H, Sampath AP, Laughlin SB, Fain GL. ATP consumption by mammalian rod photoreceptors in darkness and in light. *Curr Biol* 2008;**18**:1917-21
45. Sun P, Li H, Lu Z, Su X, Ma Z, Chen J, Li L, Zhou C, Chen Y, Chai X. Comparison of cortical responses to the activation of retina by visual stimulation and transcorneal electrical stimulation. *Brain Stimul* 2018;**11**:667-75
46. Kurimoto T, Oono S, Oku H, Tagami Y, Kashimoto R, Takata M, Okamoto N, Ikeda T, Mimura O. Transcorneal electrical stimulation increases chorioretinal blood flow in normal human subjects. *Clin Ophthalmol (Auckland, NZ)* 2010;**4**:1441-6

(Received September 19, 2019, Accepted December 16, 2019)